Spatiotemporal electron dynamics in radio-frequency glow discharges: fluid versus dynamic Monte Carlo simulations

Dimitris P Lymberopoulos and Demetre J Economou

Plasma Processing Laboratory, Department of Chemical Engineering, University of Houston, Houston, TX 77204-4792, USA

Abstract. A particle-in cell/dynamic Monte Carlo simulation technique was developed to study the spatiotemporal electron dynamics in radio-frequency glow discharges. The electric field profile in a parallel plate one-dimensional geometry was obtained from a self-consistent fluid simulation. Using this profile, the particle-in-cell/dynamic Monte Carlo simulation yielded the spatiotemporal electron velocity distribution function between the electrodes. A strongly electronegative chlorine discharge and an electropositive argon discharge were considered. At a pressure of 100 mTorr, the distribution function was non-Maxwellian except at the midgap of the chlorine discharge. The tail of the distribution was strongly modulated inside the sheath. Electron 'pile-ups' near the walls, charge double layers and negative plasma potential during part of the cycle were observed in the electronegative discharge at 13.56 MHz. Time-average results from the particle-in-cell/dynamic Monte Carlo simulation matched the fluid simulation favourably, even at a local Knudsen number $Kn \simeq 1$, with differences confined mainly to the volume around the plasma/sheath interface.

1. Introduction

Much attention has recently been paid to modelling and simulation of low-pressure glow discharge plasmas of the type used for electronic materials processing. One of the central goals of these simulations is to describe the non-equilibrium transport and reaction of the electrons accurately. Electrons are the heart of the plasma. They sustain the plasma by ionizing neutral atoms and molecules, thereby producing new electrons to counterbalance losses of electrons. In addition, electrons create reactive radicals by electron-impact dissociation of molecules. Radicals and ions are responsible for the chemistry happening on the surface of semiconductor wafers. In order to determine the rate of production of ions and radicals as a function of space and time in the reactor, one needs to know the spatiotemporal variations in the electron velocity distribution function (EVDF). Since electrons are light particles, electrons can respond to the variations of the applied RF (typically 13.56 MHz) field. Therefore, description of the electron dynamics is essential for understanding glow discharge plasmas.

There have been many studies of electron transport in low-pressure gases. In drift tube investigations, the electron swarm parameters (drift velocity, mobility and rate coefficients for electron-impact reactions) in a specified gas are studied under the influence of a given constant electric field. Such studies have been used to derive a consistent set of cross sections for electron–gas molecule collisions. Numerical simulations of drift tube experiments use finite-difference or finite-element solutions to the Boltzmann equation to determine the EVDF and in turn the swarm parameters (Pitchford and Phelps 1982, Shimura and Makabe 1992). Other investigators have used Monte Carlo methods (Hunter 1977, Reid 1979, Reid and Hunter 1979) to describe the electron collisions. In these studies the EVDF is space- and time-invariant, and the electron motion is not coupled to the ion motion since the charge density is too low for the system to be a plasma.

In glow discharge plasmas, the electron motion is intimately coupled with that of positive and negative ions. Here the electric field distribution is not known *a priori* but must be found self-consistently. There are two general approaches for simulating glow discharges; namely fluid and kinetic simulations. Fluid simulations have provided much insight into the spatiotemporal plasma flow in one-dimensional (Graves and Jensen 1986, Park and Economou 1990, Meyyappan and

Govindan 1991) as well as two-dimensional geometries (Lymberopoulos and Economou 1993b, Young and Wu 1993a, b, Dalvie *et al* 1993). The fluid equations for particle continuity, momentum and energy are obtained from the Boltzmann equation as moments of the velocity distribution function. However, fluid simulations do not resolve the particle distribution functions. Kinetic simulations such as the particle-in-cell with Monte Carlo collisions (PIC/MCC) do resolve the distribution functions (Birdsall 1991, Surendra and Graves 1991). Hybrid fluid-kinetic approaches have also been followed (Sommerer and Kushner 1992, Sato and Tagashira 1991, Ventzek *et al* 1994). Self-consistent simulations use the Poisson equation or the Maxwell equations to calculate the induced fields.

Other investigators have focused on electron transport only, using an assumed electric field distribution (not necessarily the self-consistent field). 'In that way the non-equilibrium transport of electrons, especially in the sheath region, was studied using Monte Carlo simulations (Moratz *et al* 1987, May *et al* 1993). Self-consistent Monte Carlo simulations have also been reported (Dalvie *et al* 1992a, Okuno *et al* 1992, Date *et al* 1992).

In this paper, a method of stochastic simulation, the particle-in-cell/dynamic Monte Carlo (PIC/DMC) approach, of electron transport in low-pressure glow discharge plasmas is described. The difference between PIC/DMC and the conventional PIC/MCC (Birdsall 1991), is in the way particle collisions are handled. In PIC/MCC the rather artificial null-collision method is most often applied, and the free-flight distribution of the electrons is required as an input. In PIC/DMC no time is spent in artificial (null) collisions, fewer random numbers are required per time step, and the free-flight distribution is an output of the simulation rather than an input (Lymberopoulos *et al* 1993, Lymberopoulos and Schieber 1994). The method is applied to study the electron dynamics in a glow discharge plasma sustained between two parallel plate electrodes. A strongly electronegative (chlorine) and an electropositive (argon) discharge are considered. The DMC simulation results are compared with those obtained by using a one-dimensional fluid simulation of the discharge.

2. The fluid simulation

The following assumptions were made to streamline the fluid simulation. (i) The discharge is sustained between two large parallel plate electrodes, which are separated by $L \ll R$, where R is the electrode radius. Therefore a one-dimensional description (along the direction z normal to the electrodes) of the macroscopic variables can be applied. (ii) The Cl_2 gas dissociation is negligible. (iii) No external magnetic field is applied, and the self-induced magnetic field is negligible. Therefore, Maxwell's equations reduce to the Poisson equation for the electrostatic field. (iv) The gas pressure and temperature (hence number density) are constant. (v) The ion temperature is equal to the gas temperature.

The density continuity equations for electrons, positive ions and negative ions are

$$\frac{\partial n_e}{\partial t} + \nabla \cdot J_e = \sum_j R_{ej} \tag{1}$$

$$\frac{\partial n_+}{\partial t} + \nabla \cdot J_+ = \sum_j R_{+j} \tag{2}$$

$$\frac{\partial n_-}{\partial t} + \nabla \cdot J_- = \sum_j R_{-j}. \tag{3}$$

The summation on the right-hand side of equations (1)–(3) is over all homogeneous (gas-phase) reactions creating and destroying the corresponding particle. These can be electron–neutral species, electron–ion, ion–ion and ion–neutral species. The particle fluxes are the superposition of drift under the influence of an electric field, diffusion in a concentration gradient and convection due to bulk gas flow:

$$J_e = -D_e \nabla n_e - \mu_e n_e E + v n_e \tag{4}$$

$$J_+ = -D_+ \nabla n_+ + \mu_+ n_+ E_+^{\text{eff}} + v n_+ \tag{5}$$

$$J_- = -D_- \nabla n_- - \mu_- n_- E_-^{\text{eff}} + v n_-. \tag{6}$$

The contribution of bulk gas flow (velocity v) to the total flux of charged species is generally small and was neglected.

In the so-called two-moment approach applied here, the momentum equations are simplified by neglecting the particle inertia, resulting in the drift-diffusion equations (see equations (4)–(6)). This is a good assumption for electrons, which have a fast response time due to their small mass. However, ions do not respond to the variations in the 13.56 MHz field. In order to correct for this effect while still using the drift-diffusion approximation, Richards *et al* (1987) introduced an effective electric field to which ions respond (see equations (10) and (11) below).

The electron energy balance reads

$$\frac{\partial}{\partial t}\left(\frac{3}{2} n_e k T_e\right) + \nabla \cdot q_e + e J_e \cdot E + 3 \frac{m_e}{m_+} \frac{n_e k (T_e - T_g)}{\nu_m}$$
$$+ \sum_j H_j R_j = 0 \tag{7}$$

with the total electron energy flux given by

$$q_e = -K_e \nabla T_e + \tfrac{5}{2} k T_e J_e \tag{8}$$

where the thermal conductivity of electrons is $K_e = 3k D_e n_e / 2$.

The Poisson equation relates the gradient of the electric field to the charge density:

$$\nabla \cdot E = \frac{e}{\epsilon_0} (n_+ - n_e - n_-). \tag{9}$$

Table 1. Boundary conditions used for the fluid simulation. T_{se} is the temperature of secondary electrons.

Quantity	Boundary condition
n_e	$J_e = \dfrac{1}{4}\left(\dfrac{8kT_e}{\pi m_e}\right)^{1/2} n_e \hat{n} - \gamma_+ J_+$
n_+	$J_+ = \mu_+ n_+ E_+^{eff}$, if $\hat{n} \cdot E_+^{eff} \geq 0$, otherwise $J_+ = 0$
n_{Cl^-}	$n_{Cl^-} = 0$
T_e	$q_e = \left(\dfrac{5}{2}kT_e\right)\dfrac{1}{4}\left(\dfrac{8kT_e}{\pi m_e}\right)^{1/2} n_e \hat{n} - \gamma_+ \left(\dfrac{5}{2}kT_{se}\right)J_+$
V	$V = V_{RF}\sin(2\pi ft)$ on the left-hand and $V = 0$ on the right-hand electrode, respectively

Figure 1. Electron-Cl_2 reaction rate coefficients as a function of electron energy, obtained by a zero-dimensional version of the stochastic simulation described in the text. k_m, momentum transfer; k_d, dissociative excitation to the $C^1\Pi$ state; k_{ex1}, excitation to the $B^3\Pi$ state; k_{ex2}, excitation to the $2^1\Pi$ and $2^1\Sigma$ states; k_i, ionization; k_v, vibrational excitation; k_a, attachment.

Finally, the ions respond to an effective electric field given by

$$\frac{\partial E_+^{eff}}{\partial t} = \nu_+(E - E_+^{eff}) \tag{10}$$

$$\frac{\partial E_-^{eff}}{\partial t} = \nu_-(E - E_-^{eff}). \tag{11}$$

In the above equations, n_j, J_j, D_j and μ_j ($j = e, +, -$) are particle density, flux, diffusivity and mobility, respectively. Subscripts e, + and − denote electrons, positive ions and negative ions, respectively. T_e is the electron 'temperature', E is the electric field, $E_{+(-)}^{eff}$ is the effective electric field to which ions respond, $\nu_{+(-)}$ is the positive (negative) ion–neutral species collision frequency and ε_0 is the permittivity of free space. In equation (7), the summation is over all electron–neutral species inelastic collisions. Equations (1)–(11) are written for the chlorine discharge, in which an abundance of negative ions forms. For argon, the negative ion density was set to $n_- = 0$, and equations (3), (6) and (11) were omitted.

Reactions included in the simulation were as before (Lymberopoulos and Economou 1993a, 1994). The boundary conditions are shown in table 1. In table 1, γ_+ is the secondary electron emission coefficient, and V_{RF} is the peak RF voltage applied to the electrode. These boundary conditions have been discussed elsewhere (Lymberopoulos and Economou 1994).

The rate coefficients of electron-impact reactions were calculated by solving the spatially homogeneous Boltzmann equation as a function of the electric field to neutral density ratio E/N. Calculations were performed using a zero-dimensional version of the stochastic simulation to be described in the next section. The rate coefficients as well as the average electron energy (or equivalent temperature 'T_e' were calculated as functions of E/N. These results were combined to express the rate coefficients as a function of energy (or temperature), which is one of the dependent variables (equation (7)). The result for chlorine is shown in figure 1. The rate coefficients for Ar have been presented earlier (Lymberopoulos and Economou 1993a). In that way a closure of the system of equations was obtained. This approach appears to give reasonable results (Meijer et al 1992), at least for the argon discharge, as
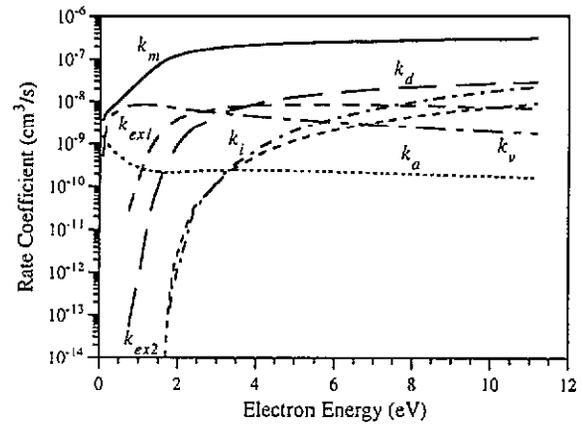
demonstrated by the quantitative predictions of our model (Lymberopoulos and Economou 1993a) as well as that of Meyyappan and Govindan (1993), both of which followed this approach.

2.1. The method of solution

The method of solution of the fluid equations has been described before (Lymberopoulos and Economou 1994). The equations were discretized in space using the Galerkin finite-element method. This way the system of partial differential equations was reduced to a system of ordinary differential equations, one for each dependent variable on each node of the finite-element mesh. Poisson's equation resulted in a system of algebraic equations. The differential/algebraic system was integrated in time until the periodic steady-state was reached. The spatiotemporal profiles of the electric field as obtained by the fluid simulation were then used in the PIC/DMC simulation described below to determine the electron velocity distribution function, as well as the spatiotemporal electron density and energy profiles.

3. The stochastic simulation

The electron velocity distribution function (EVDF) $f(r, u)$ is of paramount importance in glow discharges since the electron transport properties (hence plasma transport) and electron-impact reaction rate coefficients (hence plasma chemistry) depend on the EVDF. The EVDF can be determined by solving the Boltzmann transport equation (Holstein 1946), thus

$$\frac{\partial f}{\partial t} + u \cdot \frac{\partial}{\partial r}f + \frac{F}{m} \cdot \frac{\partial}{\partial u}f = \left(\frac{\partial f}{\partial t}\right)_{col} \tag{12}$$

where

$$\left(\frac{\partial f(r, u, \vartheta, \varphi)}{\partial t} \right)_{col}$$
$$= \sum_{j} \sum_{i} \int \int [n_j \sigma_{ij}(u', \chi) u' \delta(u - g(u', \varepsilon_{ij}, \chi))$$
$$\times f(r, u', \vartheta', \varphi') - n_j \sigma_{ij}(u, \chi) u \delta(u' - g(u, \varepsilon_{ij}, \chi))$$
$$\times f(r, u, \vartheta, \varphi)] \, du' \, d\Omega \tag{13}$$

which is a continuity equation in phase space (r, u), where r is the spatial location vector and u is the electron velocity vector. $F = q(E + u \times B)$ is the force acting on the electrons, where E and B are the electric field and magnetic induction, respectively, and m is the electron mass. The right-hand side (RHS) of equation (12) is the so-called collision integral, which can be expressed (Dalvie *et al* 1992b) as shown in equation (13). For convenience, the velocities are expressed in spherical coordinates, where u, ϑ and φ represent the electron speed, polar and azimuthal angle respectively. Equation (13) assumes that electrons collide with neutral particles (that is, short-range collisions) with velocity much lower than the electron velocity. This is an excellent assumption under the conditions of interest. The collision integral describes the discontinuous change in the EVDF due to collisions of electrons with species j, which populate (the first term within brackets on the RHS of equation (13)) or depopulate (the second term within brackets on the RHS of equation (13)) the phase space element $dr \, du \, d\vartheta \, d\varphi$. In equation (13) n_j is the density of the collision partners (atoms, molecules and so on), and σ_{ij} is the cross section of collision type i (excitation, ionization, and so on) with particle j. The cross section depends on the electron speed u and the scattering angle χ. The Dirac delta function is defined as $\delta(s) = 1$ if $s = 0$ and $\delta(s) = 0$ if $s \neq 0$. It is included to ensure that momentum and energy are both conserved during the collision. These conservation laws require

$$g(u', \varepsilon_{ij}, \chi) := \left[u'^2 \left(1 - \frac{2m}{m_j}(1 - \cos\chi) \right) - \frac{2\varepsilon_{ij}}{m} \right]^{1/2} \tag{14}$$

where m_j is the mass of particle j and ε_{ij} is the energy lost by the electron due to inelastic collision of type i with particle j. The quantity $g(u', \varepsilon_{ij}, \chi)$ is the post-collision electron speed.

The distribution function is normalized such that the integral over the phase space gives the total number of electrons n_e:

$$n_e(r) = \int \int \int f(r, u, \vartheta, \varphi) \, du \, d\vartheta \, d\varphi. \tag{15}$$

The left-hand side of equation (12) describes the flight of electrons between collisions (free flight). The velocity and position of the electrons can be calculated by using the *deterministic* relations

$$u(t_0 + \Delta t) = u(t_0) + \frac{1}{m} \int_{t_0}^{t_0 + \Delta t} F(t) \, dt \tag{16}$$

$$r(t_0 + \Delta t) = r(t_0) + \int_{t_0}^{t_0 + \Delta t} u(t) \, dt \tag{17}$$

where Δt is a sufficiently small time increment, limited by the process with the highest collision frequency, or by the requirement that an electron should not traverse a spatial cell in one time step (the Courant–Friedrich–Lewy condition).

Equation (13) is the starting point of the *stochastic* simulation. The integrals on the RHS of equation (13) can be performed by taking advantage of the following transformation of variables:

$$\delta(u - g(u', \varepsilon_{ij}, \chi)) = \left(\frac{\partial g}{\partial u'} \right)^{-1} \delta(g'(u, \varepsilon_{ij}, \chi) - u') \tag{18}$$

where $g'(u, \varepsilon_{ij}, \chi)$ represents the electron speed before the collision and has a form similar to that of equation (14) (replace u' by u and m with $-m$). Then by (i) inserting equation (18) into equation (13) and performing the integration over du', with the z axis pointing in the direction of u and (ii) integrating over time from t_0 to $t_0 + \Delta t$, whereby the electron probability density function is expanded in a Taylor's series about t_0, we obtain

$$f(r, u, 0, 0; t_0 + \Delta t | r_0, u_0, \vartheta_0, \varphi_0; t_0)$$
$$= f(r, u, 0, 0; t_0 | r_0, u_0, \vartheta_0, \varphi_0; t_0)$$
$$\times \left(1 - \Delta t \sum_{i,j} n_j u_0 2\pi \int_0^{\pi} \sigma_{ij}(u_0, \chi) \sin\chi \, d\chi \right)$$
$$+ \Delta t \sum_{i,j} n_j g'(u)$$
$$\times \int_0^{2\pi} \int_0^{\pi} \sigma_{ij}(g'(u), \chi) \left(\frac{\partial g(u')}{\partial u'} \right)^{-1}_{u'=g'(u)}$$
$$\times f(r, g'(u), \chi, \varphi' | r_0, u_0, \vartheta_0, \varphi_0) \, d\chi \, d\varphi' \tag{19}$$

where f is interpreted as a conditional probability function (van Kampen 1992) normalized to the total electron number N_e. By definition the conditional probability is

$$f(r, u, \vartheta, \varphi; t_0 | r_0, u_0, \vartheta_0, \varphi_0; t_0)$$
$$= \delta(r - r_0)\delta(u - u_0)\delta(\vartheta - \vartheta_0)\delta(\varphi - \varphi_0)N_e. \tag{20}$$

On inserting equation (20) into equation (19), making use of equation (18) and performing the integrations we obtain

$$N_e^{-1} f(r, u, 0, 0; t_0 + \Delta t | r_0, u_0, \vartheta_0, \varphi_0; t_0)$$
$$= \delta(r - r_0)\delta(u - u_0)\delta(\vartheta_0)\delta(\varphi_0)\left(1 - \sum_{i,j} \mathcal{P}_{ij}^C(u_0) \right)$$
$$+ \delta(r - r_0)\sum_{i,j} \mathcal{P}_{ij}^C(u_0)\mathcal{P}_{ij}^u(u \mid u_0)\mathcal{P}_{ij}^\chi(\vartheta_0 \mid u_0)\mathcal{P}^\varphi(\varphi_0) \tag{21}$$

where $\mathcal{P}_{ij}^C$, $\mathcal{P}_{ij}^u$, $\mathcal{P}_{ij}^\chi$ and $\mathcal{P}^\varphi$ correspond to the collision probability, the conditional probability of the electron speed, the scattering angle probability and the azimuthal

angle probability, respectively. These probabilities are defined by the following formulae:

$$\mathcal{P}_{ij}^{C}(u_0) = \Delta t \, n_j u_0 2\pi \int_0^\pi \sigma_{ij}(u_0, \chi') \sin \chi' \, d\chi' \quad (22)$$

$$\mathcal{P}_{ij}^{u}(u \mid u_0) = \delta(u - g(u_0, \varepsilon_{ij}, \chi)) \quad (23)$$

$$\mathcal{P}_{ij}^{\chi}(\chi \mid u_0) = \sigma_{ij}(u_0, \chi) \sin \chi \Big/ \int_0^\pi \sigma_{ij}(u_0, \chi') \sin \chi' \, d\chi' \quad (24)$$

$$\mathcal{P}^{\varphi}(\varphi) = 1/(2\pi). \quad (25)$$

For simplicity, the scattering and azimuthal angles ϑ_0 and φ_0 will be represented as χ and φ respectively, in the remainder of the paper. u_0 in equations (22)–(24) represents the electron speed prior to collision (the neutral species are assumed to be frozen relative to the electrons).

3.1. The simulation algorithm

An algorithm can now be devised based on equations (16) and (17) and (22)–(25) to describe the collisional motion of an electron through a given gas. In addition to knowledge of the type of gas, differential collision cross section data are needed. The trajectory of an electron in free flight is described by integrating Newton's equations of motion, equations (16) and (17). The probability that the electron will not suffer a collision is given by

$$\mathcal{P}^{NC} = 1 - \sum_{i,j} \mathcal{P}_{ij}^{C} \quad (26)$$

whereas the probability that the electron will experience a collision of type i (ionization, excitation, elastic) with particle j (atom, molecule, and so on) is given by

$$\mathcal{P}_{ij}^{C}(u_0) = \Delta t \, n_j u_0 2\pi \int_0^\pi \sigma_{ij}(u_0, \chi') \sin \chi' \, d\chi'. \quad (27)$$

A random number, r, uniformly distributed in $[0,1]$ dictates whether the electron continues its trajectory unimpeded

$$r \leqslant \mathcal{P}^{NC} \quad (28)$$

or experiences a collision of type i with particle j

$$\mathcal{P}^{NC} + \sum_{l=1}^{k-1} \mathcal{P}_l^{C} \leqslant r < \mathcal{P}^{NC} + \sum_{l=1}^{k} \mathcal{P}_l^{C} \quad (29)$$

where each value of l corresponds to a unique pair (i, j). Once the collision type has been determined, the energy of the electron is revised according to the collision characteristics (such as elastic, inelastic), by using equation (23). The velocity of the electron is then updated based on the scattering and azimuthal angles, with probability distributions given by equations (24) and (25), respectively. For the simulation reported in this paper, the scattering angle distribution function used was uniform (that is, isotropic scattering).

To account for spatially dependent force fields the particle-in-cell (PIC) simulation method (Birdsall 1991, Hockney and Eastwood 1988) was employed. The space between the electrodes was divided into 100 cells, and the force was computed at the grid points defining the cells. The force on a particle was found by linearly interpolating the forces from adjacent grid points. After a particle had moved, the new location of the particle was tested to determine whether the particle had reached the electrode. The reflection (assumed specular) probability on the electrodes was set at 0.05.

To account for production and loss of electrons (such as by ionization and attachment), electrons were removed or added to maintain the number of simulated electrons within a specified range. Typically 100–300 electrons were initially assigned velocities randomly selected from a Maxwell–Boltzmann distribution having an average energy of 4 eV. Statistics were accumulated over 50–100 RF cycles.

For gases with high tendency towards attachment, such as chlorine, the classical Monte Carlo technique can be problematic, as attachment rapidly decreases the number of electrons in the ensemble. To overcome this problem, Yousfi et al (1994) introduced a fictitious ionization process with a constant collision frequency. Although this approach counterbalances the electron loss by attachment, post-processing of the results is required as the calculated swarm parameters correspond to a fictitious gas. Our approach is to introduce 'fresh' electrons—when required—with velocity components sampled from the prevailing EVDF. The EVDF itself need not be resolved accurately as this introduces a large computational overhead. The velocity components of the seed electrons, however, reflect the EVDF as they are subject to the same underlying stochastic process. In this approach the EVDF is not perturbed, no artificial processes are introduced and the results do not require post-processing.

As electrons were moved forward in time, their velocity components were recorded at specific times in the RF cycle (phase angle ϕ), and statistics were accumulated. Numerically, the time-dependent electron energy distribution function (EEDF), $f(\varepsilon; \phi, z)$, was computed on discrete volume elements $\Delta\varepsilon_i \, \Delta\phi_j \, \Delta z_k$ located around ε_i, ϕ_j and z_k. As the simulation advanced in time the appropriate $(\varepsilon_i, \phi_j, z_k)$ bins of the EEDF were updated. The spatio-temporal electron-impact rate coefficients $k_{ij}(\phi, z)$ were obtained by numerically computing the integral

$$k_{ij}(\phi, z) = \left(\frac{2}{m}\right)^{1/2} \int_0^\infty \sigma_{ij}(\varepsilon) f(\varepsilon; \phi, z) \sqrt{\varepsilon} \, d\varepsilon. \quad (30)$$

In practice, the rate coefficients were computed by directly integrating over the EEDF. Our stochastic simulation uses the same underlying stochastic process implied by the time-dependent Boltzmann equation to generate an ensemble of realizations. Therefore, ensemble averages can be used to calculate the quantities of interest (such as electron-impact rate coefficients
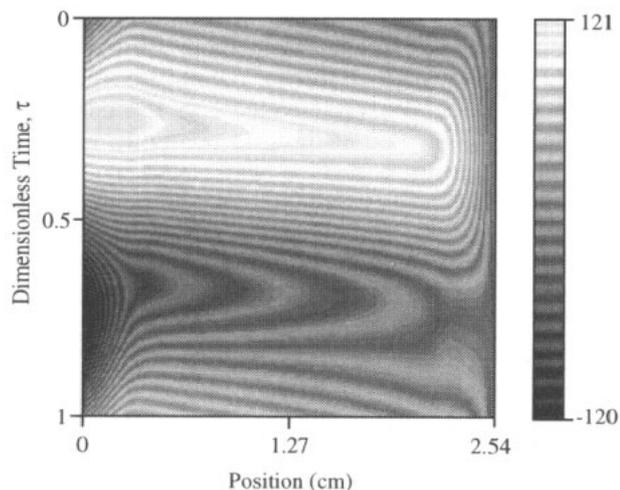
Figure 2. The spatiotemporal variation of potential in the chlorine discharge as obtained by the fluid simulation.

and electron energy), which reduces the computational burden of resolving the EEDF. The DMC simulation provided all electron-impact rate coefficients as a function of space between the electrodes and phase in the RF cycle. Because the ion density is three orders of magnitude lower, and the electron density is three to five orders of magnitude lower than the neutral particle density, electron–ion elastic collisions and electron–electron scattering were not included in the simulation.

The dynamic Monte Carlo (DMC) simulation method has some advantages compared with the null-collision Monte Carlo (NCMC) method (Skullerund 1968, Weng and Kushner 1990), which is widely used to calculate the EVDF. The NCMC method requires the electron free-flight distribution (FFD) as an input to the simulation. In contrast, DMC does not require knowledge of the FFD. In fact, the free-flight distribution is an output of the DMC simulation. In addition, the DMC method requires fewer random numbers per time step to describe the stochastic electron collision processes, and no artificial (null) collisions are introduced.

4. Results and discussion

4.1. Chlorine discharge

In the figures below, time t was normalized with respect to the RF period ($\tau = ft$). Time $\tau = 0$ corresponds to the positive zero crossing of the RF voltage applied to the electrode located at position $z = 0$ cm that is, at time $\tau = 0.25$ this electrode is at its peak positive potential. Results shown below are for 13.56 MHz, $N = 3.22 \times 10^{15}$ cm^{-3} (100 mTorr, 300 K), and 240 V peak-to-peak unless noted otherwise.

The spatiotemporal profiles of potential, as calculated by the fluid simulation, are shown in figure 2. The left-hand electrode is driven with a sinusoidal voltage (120 V peak) and the other electrode is earthed. A potential drop in the bulk plasma is clearly evident. This results in substantial bulk electric fields (as compared with electropositive plasmas, Park and Economou (1990)),
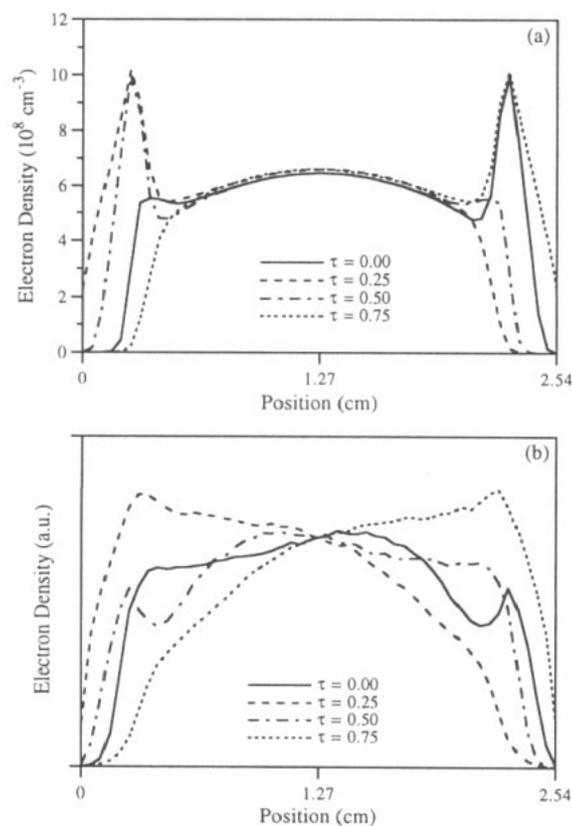

Figure 3. The spatiotemporal variation of the electron density in the chlorine discharge as obtained by (a) the fluid simulation and (b) the particle-in-cell/dynamic Monte Carlo simulation. The Monte Carlo simulation predicts only relative values of the electron density.

which are needed to carry the current through the more resistive bulk plasma. The instantaneous space potential is not always the most positive potential in the system (see for example curves near $\tau = 0.75$). However, the time-average plasma potential is positive and uniform in the bulk. Also, it is interesting to note the humps in the potential profiles near the plasma/sheath interface (such as at position about 0.45 cm at $\tau = 0.35$). These correspond to instantaneous field reversals and space-charge double layers (Gottscho 1987). In an electropositive plasma (such as argon), the whole space between the electrodes contains a net positive charge. This net charge is exceedingly small in the bulk plasma (compared with the absolute value of the individual positive ion charge) because of quasi-electroneutrality. However, the net positive charge is substantial in the sheath, which expels electrons. The situation is different in the strongly electronegative chlorine plasma in which the negative ion density far outweighs the electron density. The region right next to the electrode and that around the reactor centre-line still have a net positive charge. However, a region in between near the bulk plasma/sheath interface can have a net negative charge during part of the RF cycle. A 'double layer' then forms in the sense that a region of net positive charge is
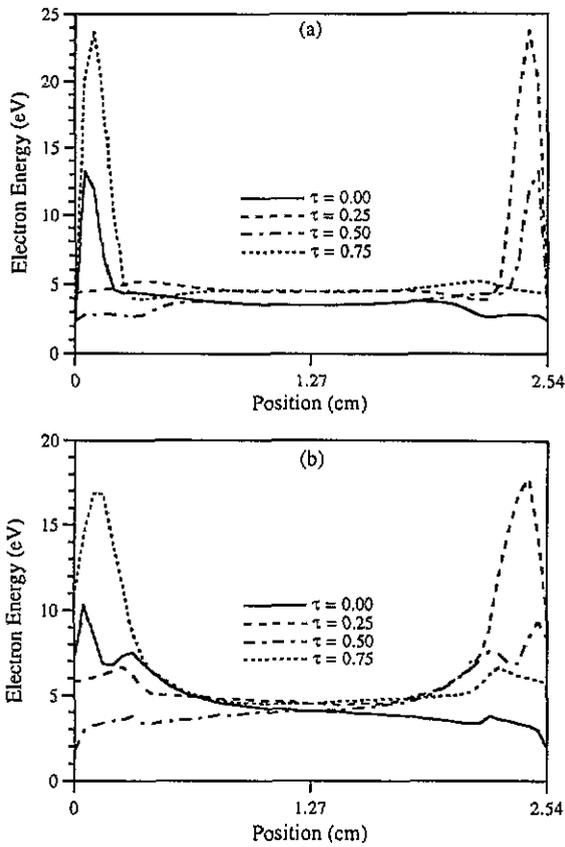
Figure 4. The spatiotemporal variation of electron energy in the chlorine discharge as obtained by (a) the fluid simulation and (b) the particle-in-cell/dynamic Monte Carlo simulation.

Figure 5. The temporal variation of the electron energy distribution function in the chlorine discharge at a distance of (a) $z = 0.3$ cm and (b) $z = 1.27$ cm from the left-hand electrode as predicted by the particle-in-cell/dynamic Monte Carlo simulation.

adjacent to another region of net negative charge. The formation of double layers may be more severe at lower frequencies (for example, 50 KHz) (Gottscho 1987), at which not only the electrons but also the ions respond to the driving frequency.

The potential difference between the plasma and the electrode (the sheath potential) is of paramount importance in these systems because it affects the ion bombardment energy. Ion–neutral species collisions in the sheath reduce the ion energy below the sheath potential and also impart an angular distribution to the ion flux bombarding the wafer. The energy and angular distribution of ions affect the shape evolution of films during etching or the microstructure and properties of deposited films. Plasma reactors currently under development operate at low pressure (0.1–50 mTorr) to enhance ion directionality, and hence avoid etching of the side-walls of microscopic features.

Figure 3(a) shows the spatiotemporal variation of the electron density distribution in the chlorine discharge as predicted by the fluid simulation. Under these conditions, the positive (and negative) ion density at the discharge centre is some 200 times higher. The electron density is modulated substantially near the electrodes, with the electrons repelled by the momentary cathode ($\tau = 0.75$, left electrode) and attracted by the momentary
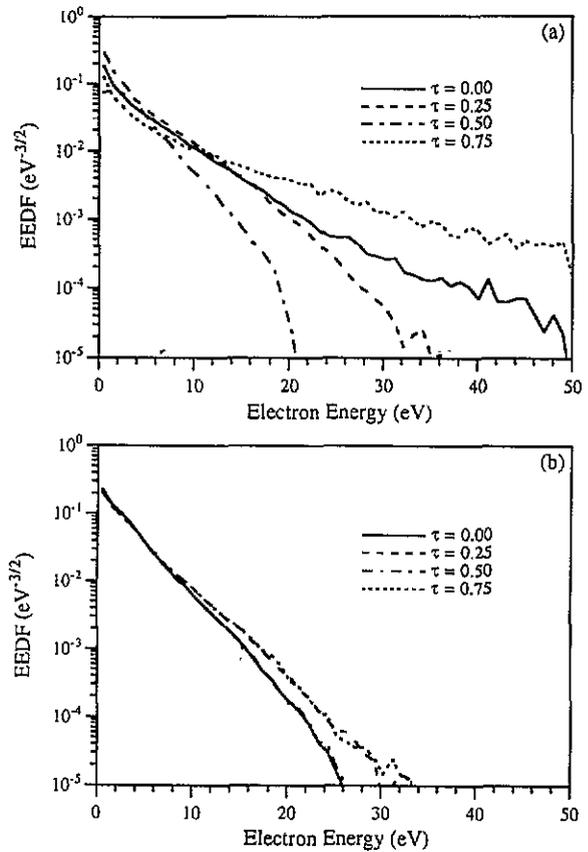
anode ($\tau = 0.25$, left electrode). Electron density modulation in the bulk of the discharge is much weaker. The electron density peaks near the bulk plasma/sheath interface. This is because of the spatiotemporal electric field distribution in the gap. There are times in the RF cycle at which the electric field crosses zero near the plasma/sheath interface. At those times electrons are repelled both from the sheath and from the bulk plasma; as a result electrons pile up near the plasma/sheath interface. Interestingly, there exists a substantial electron concentration near the wall during the anodic part of the cycle (around $\tau = 0.25$, left electrode). In essence, the sheath has to collapse to a very small thickness during that part of the cycle in order to satisfy the requirement of zero net charge flow to the wall over the RF cycle. Secondary electron emission (a value of $\gamma = 0.05$ was used) also makes a contribution to the electron density near the wall.

The electric field profiles (negative derivative of the potential shown in figure 2) obtained by the fluid simulation were used in the PIC/DMC simulation to follow the spatiotemporal electron dynamics. The electron density distribution in the gap is shown in figure 3(b). The stochastic simulation still predicts electron pile-ups near the plasma/sheath interface at the corresponding times in the RF cycle, but of much
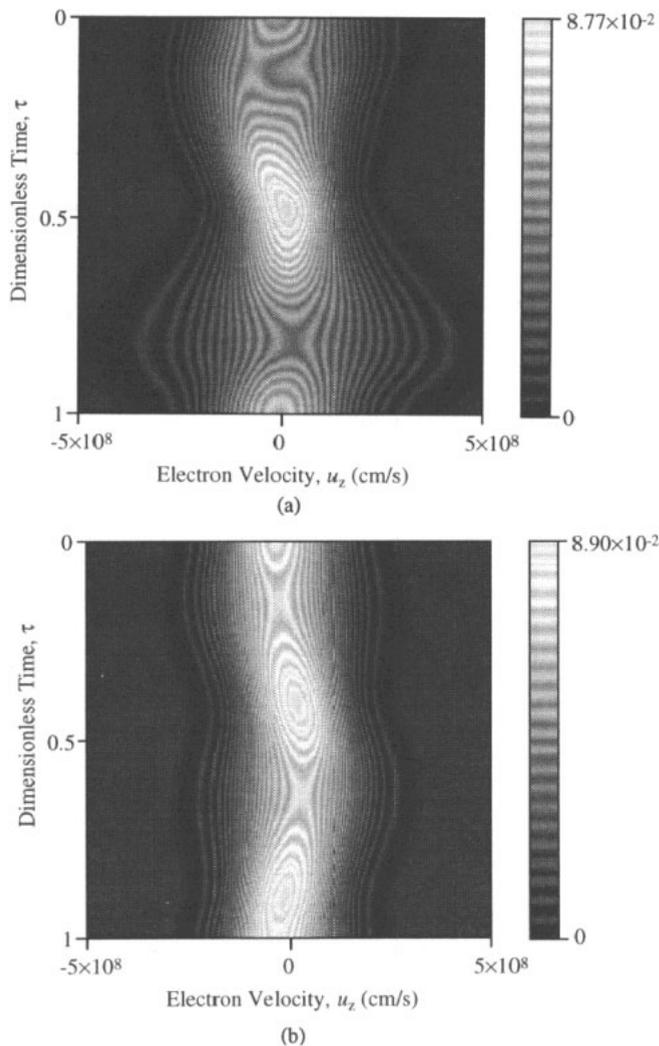
Figure 6. The distribution function of the z component of the electron velocity in the chlorine discharge at a distance of (a) $z = 0.3$ cm and (b) $z = 1.27$ cm from the left-hand electrode as predicted by the particle-in-cell/dynamic Monte Carlo simulation.
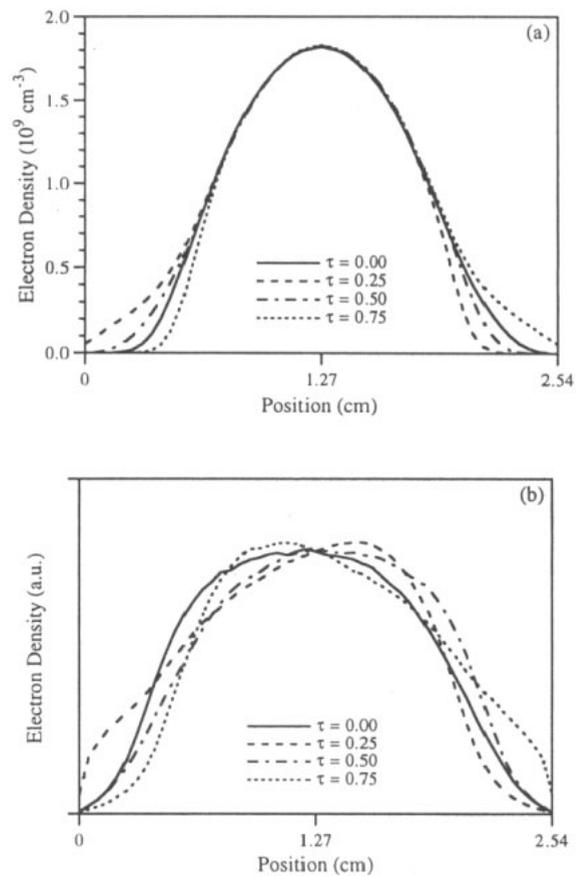

Figure 7. The spatiotemporal variation of the electron density in the argon discharge as obtained by (a) the fluid simulation and (b) the particle-in-cell/dynamic Monte Carlo simulation. The Monte Carlo simulation predicts only relative values of the electron density.

smaller magnitude than in the fluid simulation. When time-averaged, the electron density predicted by the stochastic simulation does not show local maxima near the plasma/sheath interface (see figure 10 later). Furthermore, the PIC/DMC simulation predicts a rather strong modulation of the electron density further into the bulk of the plasma.

The electron energy profiles predicted by the fluid simulation shown in figure 4(a) are compared with those predicted by PIC/DMC (figure 4(b)). The electron energy peaks in the sheath where the electric fields are higher than in the bulk plasma. Also, the electron energy is modulated strongly inside the sheath; modulation in the bulk plasma is weaker. The time-average electron temperature is nearly uniform in the bulk (see figure 11 later).

Figure 5 shows the electron energy distribution function (EEDF) in the chlorine discharge for several times in the RF cycle at a distance of (a) $z = 0.3$ cm (near the plasma/sheath interface) and (b) $z = 1.27$ cm (at the discharge centre) from the left-hand electrode. The EEDF has been normalized such that

a Maxwellian distribution would be a straight line on this semi-logarithmic plot. The EEDF has a Maxwellian character at the discharge centre, but deviations from Maxwellian form are evident near the electrode. The tail of the distribution is modulated, as the high-energy electrons have more channels available by which to lose their energy by inelastic collisions. Hence these electrons have an energy relaxation frequency higher than the applied frequency and can thus 'follow' the field. The modulation of the EEDF is much stronger near the electrode, where the electric field is much higher. Correspondingly, the tail of the distribution extends to higher energies inside the sheath.

The distribution function of the z component (normal to the electrode) of the electron velocity in the chlorine discharge is shown in figure 6, for (a) $z = 0.3$ cm (near the plasma/sheath interface) and (b) $z = 1.27$ cm (at the discharge centre) from the left-hand electrode. The time modulation of the distribution function is clearly seen. For example, the 'expansion' of the distribution to higher velocities occurs at around $\tau = 0.75$, when the electrode is at its most negative potential. Also, the modulation is more severe near the electrode. The distribution function is asymmetric with respect to the $u_z = 0$ axis, showing a net electron flux away from the electrode (distribution
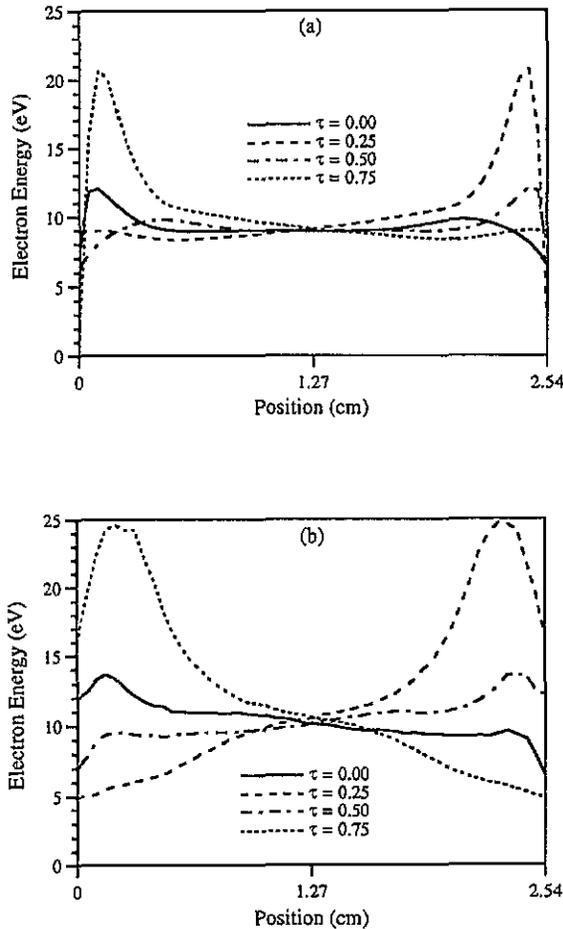
Figure 8. The spatiotemporal variation of electron energy in the argon discharge as obtained by (*a*) the fluid simulation and (*b*) the particle-in-cell/dynamic Monte Carlo simulation.

shifted towards positive u_z) or towards the electrode (distribution shifted towards negative u_z).

4.2. Argon discharge

The spatiotemporal profiles of electron density in the argon discharge are shown in figure 7(*a*) for the fluid simulation and figure 7(*b*) for the PIC/DMC simulation. The latter predicts more modulation in the bulk plasma (as in the case of chlorine, see figure 3), and also a wider density profile. This can be explained by looking at the corresponding electron energy profiles (figure 8). The PIC/DMC simulation predicts hotter electrons further away from the electrodes than does the fluid simulation. These higher energy electrons produce more ionization and fill in the wings of the electron density profile. Otherwise the electron energy profiles predicted by the two kinds of simulations look quite similar. Figures 3, 4 and 8 indicate that the non-local electron transport is more evident in the stochastic simulation than in the fluid simulation.

The temporal evolution of the EEDF near the electrode ($z = 0.3$ cm from the left-hand electrode) and at the discharge centre ($z = 1.27$ cm) as predicted by the PIC/DMC simulation are shown in figures 9(*a*) and (*b*) respectively. The EEDF near the wall appears to be
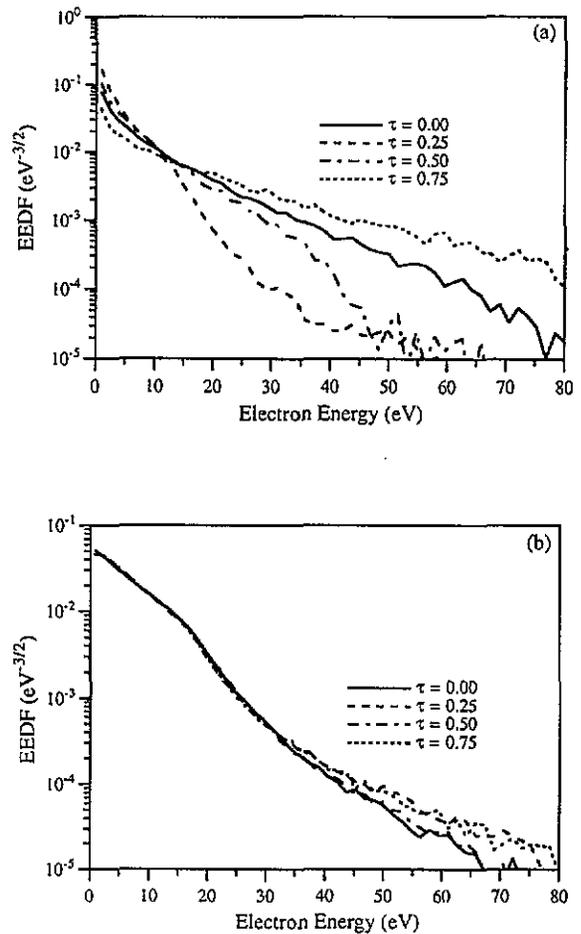
Figure 9. The temporal variation of the electron energy distribution function in the argon discharge at a distance of (*a*) $z = 0.3$ cm and (*b*) $z = 1.27$ cm from the left-hand electrode as predicted by the particle-in-cell/dynamic Monte Carlo simulation.

bi-Maxwellian, but that at the reactor centre has a non-Maxwellian character. As in the case of the chlorine discharge, the EEDF is violently modulated near the wall.

4.3. Time-average density and energy: fluid versus PIC/DMC simulations

The time-average electron density as predicted by the fluid and the PIC/DMC simulations are shown in figure 10. The stochastic simulation predicts only the relative electron density profiles; these were normalized by using the absolute electron density at $z = 1.27$ cm (the discharge centre) as predicted by the fluid simulation. One observes that there is reasonable correspondence between the fluid and stochastic simulations. In the case of Cl_2 the stochastic simulation does not predict peaks in the electron density profile near the plasma/sheath interface. It is interesting to note that the mean free path of electrons under the conditions of the simulation is about 0.25 cm, which corresponds to a Knudsen number based on the inter-electrode gap of $Kn = \lambda/L \simeq 0.1$. Using the sheath thickness as the characteristic length scale, the *local* Knudsen number is $Kn \simeq 1$. The fluid simulation (even the two-moment approach) is performing rather
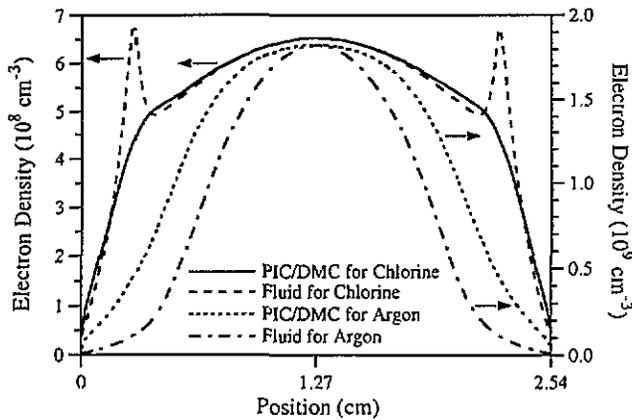
Figure 10. A comparison of time-average electron density as obtained by the fluid and particle-in-cell/dynamic Monte Carlo simulations.
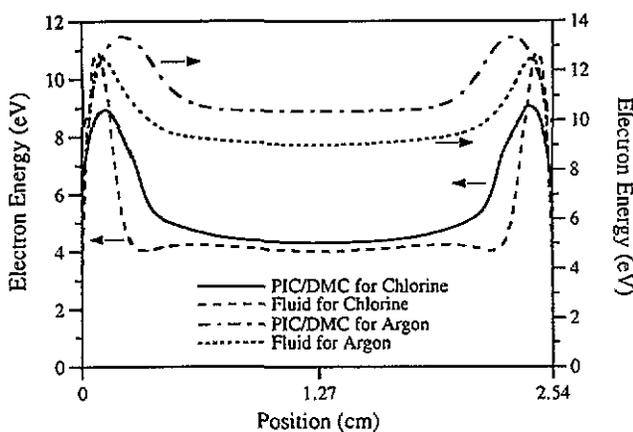

Figure 11. A comparison of time-average electron energy as obtained by the fluid and particle-in-cell/dynamic Monte Carlo simulations.

well, despite the fact that Kn is quite high and the fluid approximation may be considered suspect. In fact, recent comparisons of self-consistent particle-in-cell simulations with Monte Carlo collisions (PIC/MCC) to fluid simulations have shown that, at least for the He discharge tested (Surendra 1993), the fluid approximation gives reasonable results even at Kn > 1.

Another comparison between the PIC/DMC and the fluid simulations is shown in figure 11. The stochastic simulation predicts the absolute electron energy, so no scaling is necessary in this case. The general features of the temperature profile are captured by the fluid simulation, namely the absolute value of the electron energy, the maximum inside the sheath and the rather flat energy profile in the bulk. However, the stochastic simulation predicts a broader peak than does the fluid simulation. This may be due to the fact that constant electron transport coefficients (diffusivity, mobility) were used in the fluid simulation. Also, the fluid model may not capture the oscillating sheath (stochastic) (Godyak 1972, Turner and Hopkins 1992) heating correctly.

5. Summary

A particle-in-cell/dynamic Monte Carlo (PIC/DMC) simulation algorithm was developed to study the spatiotemporal electron dynamics in RF glow discharge plasmas. The algorithm was derived from the fundamental Boltzmann transport equation. A realistic electric field profile in a parallel plate one-dimensional geometry was obtained by a self-consistent fluid simulation of electron and ion flow in a strongly electronegative Cl_2 discharge and an electropositive Ar discharge. This electric field was used as input to the PIC/DMC simulation to obtain the spatiotemporal profiles of the electron velocity distribution function between the plates. In that sense the PIC/DMC simulation is not entirely self-consistent, since the ion motion was not followed by the kinetic simulation. The EVDF was found to deviate from Maxwellian, except at the centre of the chlorine discharge. The EVDF was modulated strongly in the 13.56 MHz field, especially the high-energy electrons, which have more channels available for energy loss and therefore a higher energy relaxation frequency.

The results from the kinetic simulation were compared with those of the self-consistent fluid simulation. In general, reasonable agreement was obtained for the electron density and energy (temperature) profiles. The differences were mostly confined to the volume around the plasma/sheath interface. This is understood since steep gradients in plasma properties appear in that region and the electron motion is influenced by the oscillating sheath. In particular, the fluid simulation may not capture any sheath 'stochastic' heating correctly. The non-local nature of the electron transport is more evident in the kinetic simulation.

The PIC/DMC simulation presented herein can be made fully self-consistent by following the ion motion as well, and using Poisson's equation to obtain the field. Also, the algorithm can be applied to arbitrary values of the Knudsen number. The purpose of this paper, however, is to present the technique rather than to conduct a detailed parametric investigation of the glow discharge. The difference between PIC/DMC and the conventional PIC/MCC (Birdsall 1991) lies in the way in which particle collisions are handled. In PIC/MCC the null-collision method is most often applied, which requires the free-flight distribution of electrons as an imput to the simulation. In PIC/DMC no time is spent in artificial (null) collisions, fewer random numbers are required per time step, and the free-flight distribution is an output of the simulation rather than an input.

Acknowledgments

References

Birdsall C K 1991 *IEEE Trans. Plasma Sci.* **19** 65–85

Dalvie M, Farouki R T, Hamaguchi S and Surendra M 1992b *J. Appl. Phys.* **72** 2620–31

Dalvie M, Hamaguchi S and Farouki R T 1992a *Phys. Rev. A* **46** 1066–77

Dalvie M, Surendra M and Selwyn G S 1993 *Appl. Phys. Lett.* **62** 3207–9

Date A, Kitamori K, Sakai Y and Tagashira H 1992 *J. Phys. D: Appl. Phys.* **25** 442–52

Godyak V A 1972 *Sov. Phys.–Tech. Phys.* **16** 1073

Gottscho R A 1987 *Phys. Rev. A* **36** 2233–42

Graves D B and Jensen K F 1986 *IEEE Trans. Plasma Sci.* **14** 78–91

Hockney R W and Eastwood J W 1988 *Computer Simulation Using Particles* (Bristol: Adam Hilger)

Holstein T 1946 *Phys. Rev.* **70** 367–84

Hunter S R 1977 *Aust. J. Phys.* **30** 83–104

Lymberopoulos D P and Economou D J 1993a *J. Appl. Phys.* **73** 3668–79

—— 1993b *Appl. Phys. Lett.* **63** 2478–80

—— 1994 *J. Vac. Sci. Technol. A* **12** 1229–36

Lymberopoulos D P, Schieber J and Economou D J 1993 *46th Gaseous Electronics Conf., Montréal, October 1993* paper MA-8 to be published

May P W, Klemperer D F and Field D 1993 *J. Appl. Phys.* **73** 1634–43

Meijer P M, Goedheer W J and Passchier J D P 1992 *Phys. Rev. A* **45** 1098–102

Meyyappan M and Govindan T R 1991 *IEEE Trans. Plasma Sci.* **19** 122–9

Meyyappan M and Govindan T R 1993 *J. Appl. Phys.* **74** 2250–9

Moratz T J, Pitchford L C and Bardsley J N 1987 *J. Appl. Phys.* **61** 2146–51

Okuno Y, Ohtsu Y and Fujita H 1992 *Japan. J. Appl. Phys.* **31** 1194–8

Park S-K and Economou D J 1990 *J. Appl. Phys.* **68** 3904–15

Pitchford L C and Phelps A V 1982 *Phys. Rev. A* **25** 540–54

Reid I D 1979 *Aust. J. Phys.* **32** 231–54

Reid I D and Hunter S R 1979 *Aust. J. Phys.* **32** 255–9

Richards A D, Thompson B E and Sawin H H 1987 *Appl. Phys. Lett.* **50** 492–4

Sato N and Tagashira H 1991 *IEEE Trans. Plasma Sci.* **19** 102–12

Shimura N and Makabe T 1992 *J. Phys. D: Appl. Phys.* **25** 751–60

Skullerud H R 1968 *J. Phys. D: Appl. Phys.* **1** 1567–8

Sommerer T J, Hitchon W N G and Lawler J E 1989 *Phys. Rev. A* **39** 6356–66

Surendra M 1993 *46th Gaseous Electronics Conf., Montréal* paper MA-1

Surendra M and Graves D B 1991 *IEEE Trans. Plasma Sci.* **19** 144–57

Turner M M and Hopkins M B 1992 *Phys. Rev. Lett.* **69** 3511–4

van Kampen N G 1992 *Stochastic Processes in Physics and Chemistry* 2nd edn (Amsterdam: North Holland)

Ventzek P L G, Hoekstra R J and Kushner M J 1994 *J. Vac. Sci. Technol. B* **12** 461–77

Weng Y and Kushner M J 1990 *Phys. Rev. A* **42** 6192–200

Young F F and Wu C-H 1993a *J. Appl. Phys.* **74** 839–47

—— 1993b *Appl. Phys. Lett.* **62** 473–5

Yousfi M, Hennad A and Alkaa A 1994 *Phys. Rev. E* **49** 3264–73